JBC RESEARCH ARTICLE

Cataract-linked serine mutations in the gap junction protein connexin50 expose a sorting signal that promotes its lysosomal degradation

Received for publication, December 14, 2021, and in revised form, January 21, 2022 Published, Papers in Press, February 2, 2022,
https://doi.org/10.1016/j.jbc.2022.101673

Peter J. Minogue[1], Jun-Jie Tong[2], Kelly Wichmann[1], Hubert Mysliwiec[1], Lisa Ebihara[2,3], Eric C. Beyer[1], and Viviana M. Berthoud[1,*]

From the [1]Department of Pediatrics, University of Chicago, Chicago, Illinois, USA; [2]Center of Proteomics and Molecular Therapeutics, and [3]Discipline of Physiology and Biophysics, Rosalind Franklin University of Medicine and Science, North Chicago, Illinois, USA

Edited by Phyllis Hanson

Many human connexin50 (Cx50) mutants have been linked to cataracts including two carboxyl terminus serine mutants that are known phosphorylation sites in the lens (Cx50S258F and Cx50S259Y). To examine the behavior of these mutants and the role of phosphorylation at these positions, we stably transfected HeLa cells with cataract-linked and phosphorylation-mimicking (Cx50S258D and Cx50S259D) Cx50 mutants. We observed that gap junctional plaques were rarely detected in Cx50S258F-expressing and Cx50S259Y-expressing cells compared with wild-type cells. In contrast, gap junction abundance and size were greatly increased for Cx50S258D and Cx50S259D mutants. Cx50S258F and Cx50S259Y supported very low levels of gap junctional coupling, whereas Cx50S258D and Cx50S259D supported extensive intercellular communication. Furthermore, Cx50 levels as detected by immunoblotting were lower in Cx50S258F and Cx50S259Y mutants than in the wild-type or the aspartate substitution mutants, and chloroquine or ammonium chloride treatment significantly increased Cx50S258F and Cx50S259Y protein levels, implying participation of the lysosome in their increased degradation. Alanine substitution of amino acids within a predicted tyrosine-based sorting signal in Cx50S258F and Cx50S259Y increased levels of gap junctional plaques and intercellular transfer of neurobiotin. These results suggest that the absence of phosphorylatable serines at these positions exposes a sorting signal leading to lysosomal degradation of Cx50, whereas phosphorylation at these sites conceals this signal and allows targeting of Cx50 to the plasma membrane and stabilization of gap junction plaques. We propose that in the lens, degradation of Cx50S258F and Cx50S259Y decreases Cx50 levels at the plasma membrane and consequently Cx50 function, leading to cataracts.

Normal organ function depends on intercellular communication facilitated by channels contained within gap junctions that allow direct intercellular diffusion of ions and small molecules up to ~1 kDa (including many intracellular signaling molecules). These channels are formed by members of a family of related integral membrane proteins called connexins. The connexins contain four transmembrane domains with the amino and carboxyl termini localized in the cytoplasm. The biological importance of connexins and the intercellular communication that they support is emphasized by the linkage of mutations in different connexin genes to diverse human diseases, including oculodentodigital dysplasia, deafness, cataracts and diseases of skin, nervous system, and cardiovascular system (reviewed in Refs. (1–3)). Studies of wild-type and mutant connexins expressed in cells or in animal models have provided a significant body of information regarding their function, life cycle, and regulation, and the contributions of the different connexin polypeptide domains to these processes.

To elucidate how alterations of connexins contribute to disease, we have been studying two connexins that are almost uniquely expressed in the lens, connexin46 (Cx46) and connexin50 (Cx50). The lens is formed by an anterior epithelial cell layer and fiber cells that comprise the bulk of the organ. The normal healthy lens is a transparent avascular organ that relies on gap junction–mediated intercellular communication to maintain homeostasis and transparency by supporting the circulation of water and ions within the organ (reviewed in Refs. (4–6)). A large number of Cx46 and Cx50 mutants have been identified in families of people with inherited congenital cataracts. Like the mutants of other connexins associated with disease, many of the cataract-linked Cx46 and Cx50 mutants do not traffic properly and are degraded or accumulate in intracellular compartments; therefore, they are unable to support intercellular communication. Some mutants traffic to the plasma membrane properly and form gap junctional plaques, but they are not functional or have altered gap junctional channel or hemichannel properties (reviewed in Ref. (7)). Many of the cataract-linked mutations that have been previously studied are missense substitutions of amino acids in the first half of the molecule (from the amino terminus through the fourth transmembrane domain). These studies have helped to elucidate specific structure–function relationships in the connexins.

* For correspondence: Viviana M. Berthoud, vberthou@peds.bsd.uchicago.edu.

Only a small number of cataract-linked mutations have been identified in the carboxyl terminal domain, even though this domain corresponds to a large fraction of the connexin protein (~50% for Cx50), and the mechanisms by which they lead to disease have only been studied for a few of them (8–10). The carboxyl terminus of all connexins is located within the cytoplasm and has been implicated in various protein–protein interactions (reviewed in Refs. (11, 12)). It contains many sites for post-translational modification (among which phosphorylation is prominent). The post-translational modifications and protein–protein interactions can influence several aspects of the connexin life cycle and channel physiology (reviewed in Refs. (11, 12)).

In the current study, we characterized the cellular and functional properties of two cataract-linked Cx50 mutations, Cx50S258F and Cx50S259Y (13–15), in stably transfected HeLa cells and *Xenopus* oocyte pairs. These mutations affect adjacent serines in the carboxyl terminus of the protein (Fig. 1*A*). Mass spectrometry studies of human, bovine, and ovine lenses have shown that the serines corresponding to S258 and S259 of human Cx50 are phosphorylated (16–19). Therefore, these mutants provided an opportunity to get insights into the function of phosphorylation at these positions and how it relates to disease. Our results show that these mutants cause disease by impairing Cx50 function through exposure of a sorting signal that targets them to the lysosome, a cellular mechanism that has not previously been described for any disease-causing connexin mutant.

Results

The cataract-linked mutants, Cx50S258F and Cx50S259Y, decrease abundance of gap junctional plaques and levels of Cx50, which are restored by substituting aspartic acid

To study the behavior of Cx50S258F and Cx50S259Y, we generated stably transfected HeLa cells expressing these mutants (HeLa-Cx50S258F and HeLa-Cx50S259Y). These serines are phosphorylated in human, bovine, and ovine lenses (16–19). Therefore, to test the effect of a negative charge that mimics phosphorylation at these positions, we generated stably transfected HeLa cells expressing Cx50 in which S258 or S259 was replaced by aspartic acid (HeLa-Cx50S258D and HeLa-Cx50S259D).

To assess trafficking to the plasma membrane and formation of gap junctional plaques, we localized Cx50 by immunofluorescence. HeLa cells expressing wild-type Cx50 (HeLa-Cx50) frequently showed immunoreactive staining at gap junctional plaques and weak staining in the perinuclear region (Fig. 1*B*). In contrast, both HeLa-Cx50S258F and HeLa-Cx50S259Y cells showed Cx50 immunoreactivity in the

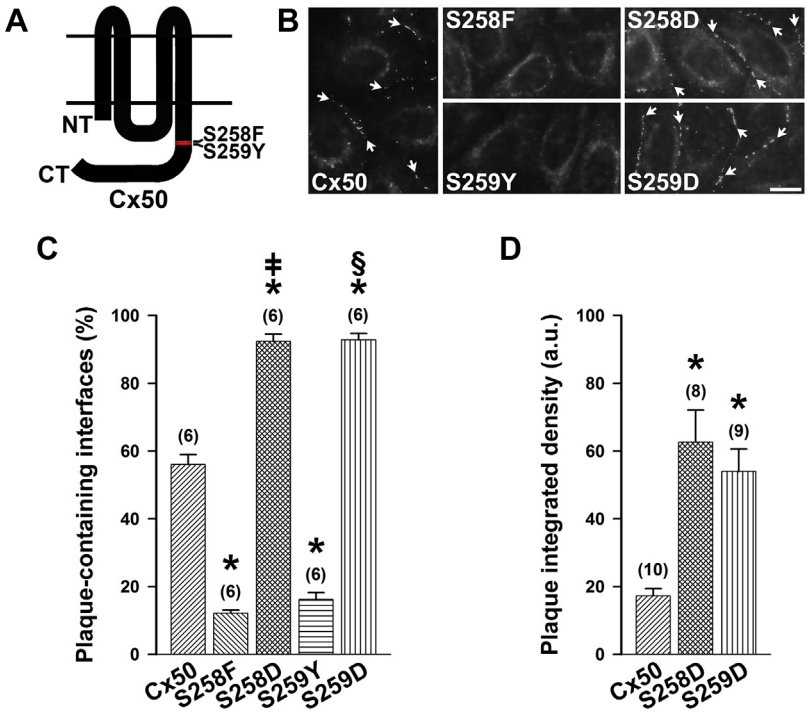

Figure 1. Gap junction abundance is decreased in HeLa-Cx50S258F and HeLa-Cx50S259Y cells. *A*, the diagram depicts the membrane topology of Cx50 and the localization of the mutated serines in the carboxyl terminus of the protein. The plasma membrane boundary is indicated by the *horizontal lines*. *B*, photomicrographs show the distribution of immunoreactive Cx50 in HeLa cells stably transfected with Cx50, Cx50S258F (S258F), Cx50S258D (S258D), Cx50S259Y (S259Y), or Cx50S259D (S259D). *Arrows* point to gap junctional plaques at cell interfaces. The scale bar represents16 μm. *C*, graph shows the percentage of cell interfaces containing gap junctional plaques in HeLa-Cx50, HeLa-Cx50S258F, HeLa-Cx50S258D, HeLa-Cx50S259Y, and HeLa-Cx50S259D cells (as the mean [bar] + SEM [error bar]). ‡ indicates a significant difference between HeLa-Cx50S258F and HeLa-Cx50S258D cells, and § indicates a significant difference between HeLa-Cx50S259Y and HeLa-Cx50S259D cells. *D*, graph depicts the integrated density of the gap junctional plaques (as the mean [bar] + SEM [error bar]) in HeLa-Cx50, HeLa-Cx50S258D, and HeLa-Cx50S259D in arbitrary units (a.u.). Significant differences *versus* HeLa-Cx50 cells are indicated by *asterisks* in *C* and *D*. The number of microscopic fields analyzed (statistical n) is indicated within parentheses. CT, carboxyl terminus; Cx50, connexin50; NT, amino terminus.

perinuclear region (Fig. 1*B*), and, very rarely, they showed some small plaques at membrane appositions that were weakly stained (not shown). The number of membrane interfaces containing gap junctional plaques was 56% in HeLa-Cx50 cells, but it was significantly less in HeLa-Cx50S258F cells (12%) and HeLa-Cx50S259Y cells (16%) (Fig. 1*C*). In contrast, cells expressing the aspartate substitution mutants showed abundant and strong staining of gap junctional plaques (Fig. 1*B*). The percentage of cell interfaces containing gap junctional plaques was 92% in HeLa-Cx50S258D cells and 93% in HeLa-Cx50S259D cells *versus* 56% in HeLa-Cx50 cells (Fig. 1*C*). Moreover, the integrated density of immunoreactive gap junctional plaques (area × fluorescence intensity) in the cells expressing the aspartate substitution mutants was 3.6 times (for Cx50S258D) and 3.1 times (for Cx50S259D) the value determined in HeLa cells expressing wild-type Cx50 (Fig. 1*D*).

The perinuclear distribution of the cataract-linked mutants suggested that they localized predominantly in the Golgi compartment. To test this, we performed double-label immunofluorescence with anti-Golgi 58K and anti-Cx50 antibodies in HeLa cells expressing wild-type Cx50 or the Cx50 mutants. Some wild-type Cx50 colocalized with the Golgi marker, but Cx50S258F and Cx50S259Y showed a distribution similar to the Golgi 58K protein (Fig. S1). Treatment of the cells with brefeldin A (a compound that collapses the Golgi apparatus into the endoplasmic reticulum) resulted in redistribution of Cx50 as expected. After brefeldin A treatment of HeLa-Cx50S258F and HeLa-Cx50S259Y cells, Cx50 distributed throughout the cell as did the Golgi 58K protein. Brefeldin A-treated HeLa-Cx50 cells showed redistribution of intracellular staining and a few remaining Cx50 gap junctional plaques (Fig. S1).

We determined Cx50 levels in the HeLa transfectants by immunoblotting. Levels of Cx50 were significantly lower in HeLa-Cx50S258F and HeLa-Cx50S259Y cells compared with those in HeLa-Cx50 cells (61% and 20% *versus* Cx50, respectively; Fig. 2, *A* and *B*). In contrast, levels of Cx50 in HeLa-Cx50S258D and HeLa-Cx50S259D cells were not significantly different from cells expressing wild-type Cx50 (1.72 and 2.13 times the value in HeLa-Cx50 cells, respectively; $p > 0.05$). However, these levels differed from those determined in the HeLa cells expressing the corresponding cataract-linked mutants. In HeLa-Cx50S258D cells, protein levels of Cx50 were 2.3 times the levels in HeLa-Cx50S258F, and, in HeLa-Cx50259D, they were 10.8 times the levels in HeLa-Cx50S259Y (Fig. 2, *A* and *B*). To test whether these differences could result from changes in mRNA levels, we performed reverse transcription quantitative PCR. Cx50 mRNA levels were similar between the HeLa cells expressing wild-type Cx50 and cells expressing the cataract-linked mutant, Cx50S258F (Fig. 2*C*). Cx50 mRNA levels were significantly lower in HeLa-Cx50S259Y cells compared with HeLa-Cx50 cells (Fig. 2*D*), but the change was much less than that of Cx50 protein levels (about 1/2 *versus* 1/5 for the protein levels). The increased Cx50 levels in HeLa cells expressing the aspartate substitution mutants did not result from changes in transcript levels; Cx50 mRNA levels were similar between HeLa-Cx50S258D and HeLa-Cx50S258F cells and between HeLa-Cx50S259D and HeLa-Cx50S259Y cells (Fig. 2, *C* and *D*). These results suggested that the reduced Cx50 levels in cells expressing the cataract-linked Cx50 mutants resulted from degradation of the protein.

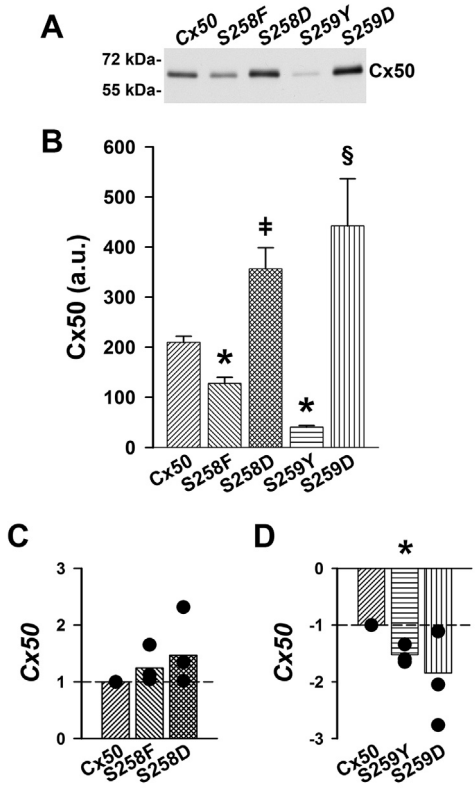

Figure 2. Levels of Cx50 are decreased in HeLa-Cx50S258F and HeLa-Cx50S259Y cells. *A*, immunoblot of Cx50 in homogenates from HeLa cells stably transfected with Cx50, Cx50S258F (S258F), Cx50S258D (S258D), Cx50S259Y (S259Y), or Cx50S259D (S259D). The migration positions of the molecular mass markers are indicated on the *left*. *B*, graph shows the mean (bar) + SEM of the densitometric values of the immunoreactive bands obtained from three independent experiments expressed in arbitrary units (a.u.). ‡ indicates a significant difference between HeLa-Cx50S258F and HeLa-Cx50S258D cells, and § indicates a significant difference between HeLa-Cx50S259Y and HeLa-Cx50S259D cells. *C* and *D*, graphs show the levels of Cx50 transcripts in HeLa-Cx50S258F and HeLa-Cx50S258D (*C*) and HeLa-Cx50S259Y and HeLa-Cx50S259D (*D*) cells relative to the levels in HeLa-Cx50 cells as determined by reverse transcription quantitative PCR. The bars represent the geometric mean of the relative levels obtained in three independent experiments (*filled circles*). The value obtained in HeLa-Cx50 cells was considered as the reference (*short dashed line* at fold change = +1 in *A* and −1 in *B*). *Asterisks* denote significant differences *versus* HeLa-Cx50 cells. Cx50, connexin50.

The cataract-linked Cx50 mutants are degraded by the lysosome

Both the proteasome and the lysosome have been implicated in degradation of wild-type and mutant connexins (reviewed in Refs. (20, 21)). To test whether these organelles were involved in the degradation of the Cx50 mutants, we treated HeLa cell transfectants with epoxomicin (a proteasome inhibitor), chloroquine (a lysosomotropic amine that inhibits the activity of lysosomal enzymes by increasing the pH of the lysosome), or NH_4Cl (a lysosomotrophic neutralizing agent).

Treatment of HeLa-Cx50, HeLa-Cx50S258F, HeLa-Cx50S259Y, HeLa-Cx50S258D, and HeLa-Cx50S259D cells with epoxomicin for 4 h did not lead to a significant increase in levels of immunoreactive Cx50 in any of the HeLa cell transfectants (Fig. S2). Contrary to the expectation, Cx50S259Y levels were decreased ($p < 0.025$, n = 3). Inhibition of the proteasome pathway was confirmed by immunoblotting, which showed increased abundance of ubiquitinated proteins (Fig. S3).

Chloroquine treatment induced a large increase of Cx50 levels in the cells expressing the cataract-associated mutants (74% for Cx50S258F and 62% for Cx50S259Y above the levels in untreated cells; $p < 0.004$, n = 3). Chloroquine treatment led to smaller increases in cells expressing wild-type Cx50 (44%; $p < 0.01$, n = 7), Cx50S258D (26%; $p < 0.03$, n = 3), and Cx50S259D (18%; $p < 0.05$, n = 9) (Fig. 3, *A* and *B*). Similarly, treatment with NH_4Cl induced an increase in Cx50 levels in all transfectants. The increment was greatest in cells expressing the cataract-linked mutants (Fig. 3, *C* and *D*); specifically, while levels of Cx50 increased 66% in HeLa-Cx50S258F cells and 65% in HeLa-Cx50S259Y cells, they increased 35% in HeLa-Cx50 cells, 31% in HeLa-Cx50S258D cells, and 47% in HeLa-Cx50S259D cells after treatment with NH_4Cl for 4 h (n = 4). Thus, mutating S258 or S259 to aspartate recovered Cx50 protein levels to wild-type values (as shown in Fig. 2, *A* and *B*) and decreased the proportion of the protein that was available for lysosomal degradation (likely by increasing its permanence at the plasma membrane).

We also examined the effects of lysosomal inhibition on the cellular localization of Cx50 in the HeLa transfectants. Immunoreactive Cx50 was present in a more punctate/vesicular pattern within the cytoplasm in cells expressing wild-type Cx50 or any of the Cx50 mutants after treatment with either chloroquine (Fig. S4) or NH_4Cl (Fig. S5), consistent with their accumulation after inhibiting lysosomal degradation. Some punctate staining at appositional membranes was still detected in cells expressing wild-type Cx50, Cx50S258D, or Cx50259D, consistent with the presence of gap junction plaques that were not yet undergoing internalization/degradation.

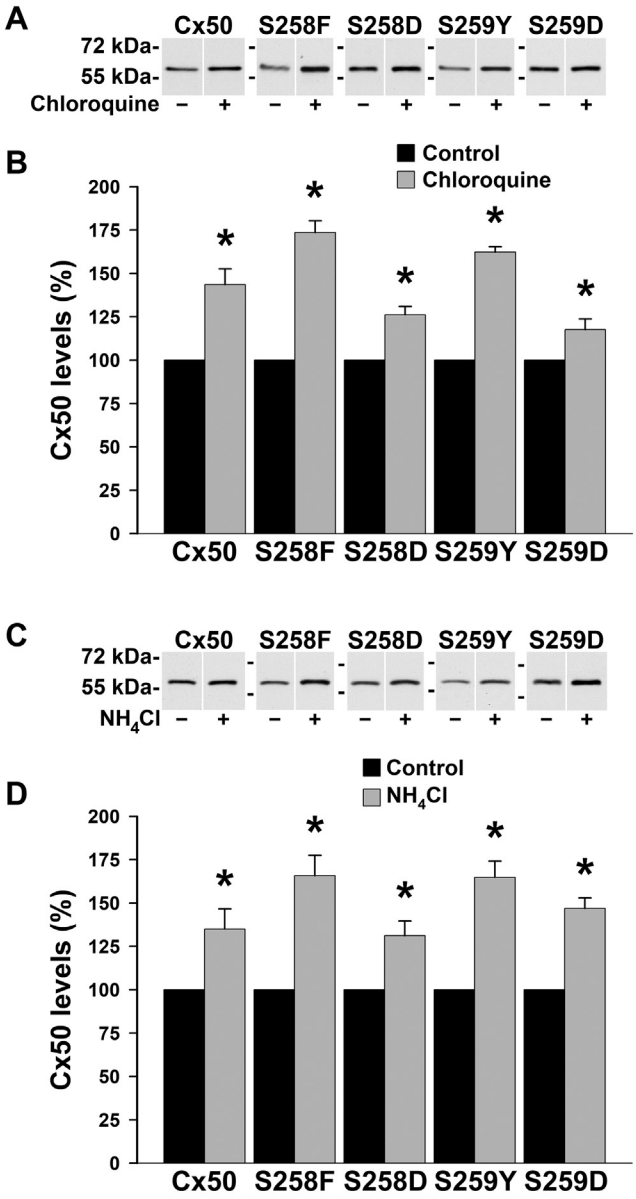

Figure 3. Lysosomal inhibitors increase levels of wild-type and mutant Cx50. *A* and *C*, immunoblots of Cx50 in homogenates from HeLa cells stably transfected with Cx50, Cx50S258F (S258F), Cx50S258D (S258D), Cx50S259Y (S259Y), or Cx50S259D (S259D) left untreated or treated with 100 μM chloroquine (*A*) or 20 mM ammonium chloride (NH_4Cl, *C*) for 4 h. The migration positions of the molecular mass markers are indicated on the *left*. (The exposure times of the X-ray films were varied for the different Cx50 transfectants to permit accurate calculation of the effects of chloroquine and NH_4Cl; therefore, direct comparisons between wild-type and mutant Cx50 levels cannot be made from these data). *B* and *D*, graphs show the mean (bar) + SEM of the densitometric values of the immunoreactive Cx50 bands obtained after treatment with chloroquine (*B*) or NH_4Cl (*D*) in at least three independent experiments expressed as a percentage of the levels in the corresponding untreated wild-type or mutant Cx50-transfected HeLa cells (for the chloroquine experiments, n = 3 for S258F, S258D, and S259Y; n = 7 for Cx50 and n = 9 for S259D; for the NH_4Cl experiments, n = 4 for all transfectants). *Asterisks* denote significant differences between the untreated control cells (*black bars*) and the corresponding chloroquine-treated or NH_4Cl-treated cells (*gray bars*). Cx50, connexin50.

The cataract-linked mutants affect Cx50 function

To test the effect of mutation of S258 and S259 on Cx50 function, we determined gap junctional conductance in pairs of *Xenopus* oocytes expressing wild-type or mutant Cx50. As expected, wild-type Cx50 induced large junctional conductances compared with control oocyte pairs injected only with oligonucleotides antisense to the endogenous *Xenopus* Cx38 (38.9 μS *versus* 0.47 μS) (Fig. 4*A*). In contrast, Cx50S259Y did not induce junctional conductances above those detected in the control oocyte pairs (1.44 μS), and Cx50S258F induced junctional conductances that were only ∼20% of the values induced by wild-type Cx50 (8.06 μS for Cx50S258F-injected oocyte pairs *versus* 38.9 μS for wild-type Cx50-injected oocyte pairs) (Fig. 4*A*). Interestingly, the aspartate substitution mutants, Cx50S258D and Cx50S259D, induced junctional conductances that were significantly higher than those induced by wild-type Cx50 (67.26 μS for Cx50S258D-injected oocyte pairs and 73.72 μS for Cx50S259D-injected oocyte pairs *versus* 28.27 μS for wild-type Cx50-injected oocyte pairs) (Fig. 4*B*).

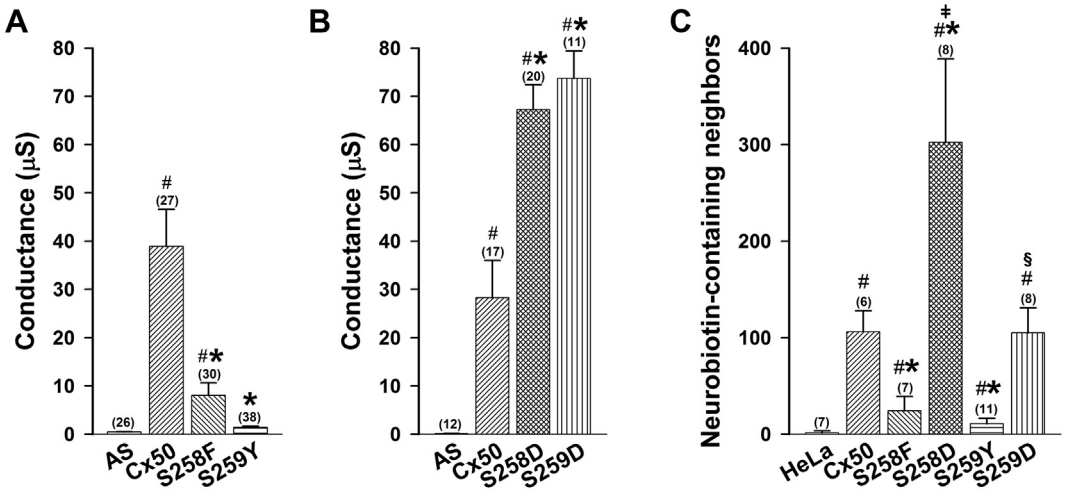

Figure 4. Intercellular communication is decreased in *Xenopus* oocytes and HeLa cells expressing the cataract-linked mutants. *A* and *B*, bar graphs show the mean gap junctional conductances determined using the double two-electrode voltage clamp technique in pairs of oocytes expressing wild-type Cx50 (*A* and *B*) or the cataract-linked mutants (*A*) or the aspartate-substitution mutants (*B*). AS indicates oocytes that were injected with no RNA (*i.e.*, they were injected with *Xenopus* Cx38 antisense oligonucleotide alone). The number of pairs tested is indicated within parentheses. # indicates significant differences with AS-injected oocytes; *asterisks* indicate significant differences with wild-type Cx50-injected oocyte pairs. *C*, bar graph shows the quantification of intercellular transfer of neurobiotin in untransfected HeLa cells (HeLa) and HeLa cells stably transfected with Cx50, Cx50S258F (S258F), Cx50S258D (S258D), Cx50S259Y (S259Y), or Cx50S259D (S259D). The results are presented as mean (bar) + SEM. *Asterisks* indicate significant differences *versus* HeLa-Cx50 cells; # indicates significant difference *versus* HeLa cells; ‡ indicates a significant difference between HeLa-Cx50S258F and HeLa-Cx50S258D cells; and § indicates a significant difference between HeLa-Cx50S259Y and HeLa-Cx50S259D cells. The number of microinjected cells is indicated within parentheses. Cx50, connexin50.

To test whether intercellular transfer of small molecules was affected in the Cx50 mutants, we studied intercellular transfer of microinjected neurobiotin in the stably transfected HeLa cells. Both Cx50S258F and Cx50S259Y supported neurobiotin transfer to a significantly higher number of neighboring cells than untransfected HeLa cells, but to a significantly lower number of cells than wild-type Cx50 (24.3 and 10.9 cells in HeLa-Cx50S258F cells and HeLa-Cx50S259Y cells *versus* 1.6 cells in untransfected HeLa cells and 106 cells in HeLa-Cx50 cells) (Fig. 4*C*). Both D-substituted mutants recovered intercellular transfer of neurobiotin; the number of neurobiotin-recipient cells was similar (105 cells in HeLa-Cx50S259D cells) or greater (302.3 cells in HeLa-Cx50S258D cells) than that among cells expressing wild-type Cx50 (Fig. 4*C*).

The C terminus of Cx50 contains a sorting signal

Because introduction of a negative charge at amino acid positions 258 or 259 that mimicked phosphorylation restored localization of the protein to gap junctional plaques and its function and, consequently, made the protein less likely to become a substrate for lysosomal degradation, we considered the possibility that the C terminus of Cx50 contained a signal that regulated its subcellular trafficking. This sorting signal might become exposed by the cataract-linked mutations, which remove these seryl phosphorylation sites. Therefore, we searched the amino acid sequence of the C terminus of Cx50 for consensus sorting signals. We identified several sequences that conform to the tyrosine-based sorting signal of the YXXΦ type in which Y is tyrosine, X is any amino acid, and Φ is an amino acid with a bulky hydrophobic side chain (*e.g.*, F, M, L, I, or V) (reviewed in Ref. (22)): Y^{266}QLL, Y^{278}FPL, and Y^{323}AQV.

To test the hypothesis that one of these sorting signals was involved in making the cataract-linked Cx50 mutants extremely susceptible to lysosomal degradation, we initially generated mutants of Cx50S258F and Cx50S259Y in which amino acids 261 to 279 were deleted (Δ261–279). When we screened batch clones of HeLa cells transfected with these mutants by immunofluorescence, we observed the presence of abundant gap junctional plaques at appositional membranes (Fig. S6). This result suggested that a sorting sequence was localized between amino acids 261 to 279 (and it excluded involvement of the sequence Y^{323}AQV as a putative signal).

Because tyrosine is an absolute requirement in this type of sorting signal, and it cannot be replaced by any other amino acid, we generated mutants to destroy the putative sorting signals between amino acids 261 and 279 in Cx50S258F and Cx50S259Y by replacing Y^{266} or Y^{278} with alanine (Y266A and Y278A). As a first approach, we obtained batch clones of HeLa cells expressing these constructs and screened them for the presence of gap junctional plaques by immunofluorescence. While abundant gap junctional plaques were observed in cells expressing Cx50S258F–Y266A and Cx50S259Y–Y266A, replacement of Y^{278} by alanine did not increase gap junction abundance (not shown). This implicated Y^{266}QLL, but not Y^{278}FPL, in the increased lysosomal sorting of the mutant Cx50. We also replaced L^{268} and L^{269} with alanines (Cx50S258F–L268A–L269A and Cx50S259Y–L268A–L269A) because this type of sorting signal also requires an amino acid with a bulky hydrophobic side chain at position 4. When we screened batch clones of HeLa cells expressing these alanine substitution mutants, we observed abundant gap junctional plaques. Taken together, these results suggested that the Y^{266}QLL signal was responsible for the behavior of the

cataract-linked mutants. Therefore, for quantitative analysis, we generated clones of stably transfected HeLa cells expressing the following mutants: Cx50S258F–Y266A, Cx50S258F–L268A–L269A, Cx50S259Y–Y266A, and Cx50S259Y–L268A–L269A (Fig. 5*A*).

HeLa cells stably transfected with the Y266 and L268–L269 alanine-substitution mutants of Cx50S258F or Cx50S259Y had numerous strongly immunostained gap junctional plaques (Fig. 5*B*). The percentage of plasma membrane interfaces containing gap junctional plaques in cells transfected with the alanine-substitution mutants was much greater than that in wild-type Cx50 HeLa cell transfectants (87% for HeLa-Cx50S258F–Y266A cells, 92% for HeLa-Cx50S258F–L268A–L269A cells, 88% for HeLa-Cx50S259Y–Y266A cells, 91% for HeLa-Cx50S259Y–L268A–L269A cells *versus* 57% for HeLa-Cx50 cells) (Fig. 5*C*). In addition, the integrated densities of immunoreactive gap junctional plaques in the cells expressing these alanine-substitution mutants were significantly higher compared with those in HeLa-Cx50 cells (Fig. 5*D*). After the alanine substitution for Y266 in Cx50258F and Cx50S259Y, the integrated densities of immunoreactive gap junctional plaques were, respectively, 4.3 and 4.5 times the value

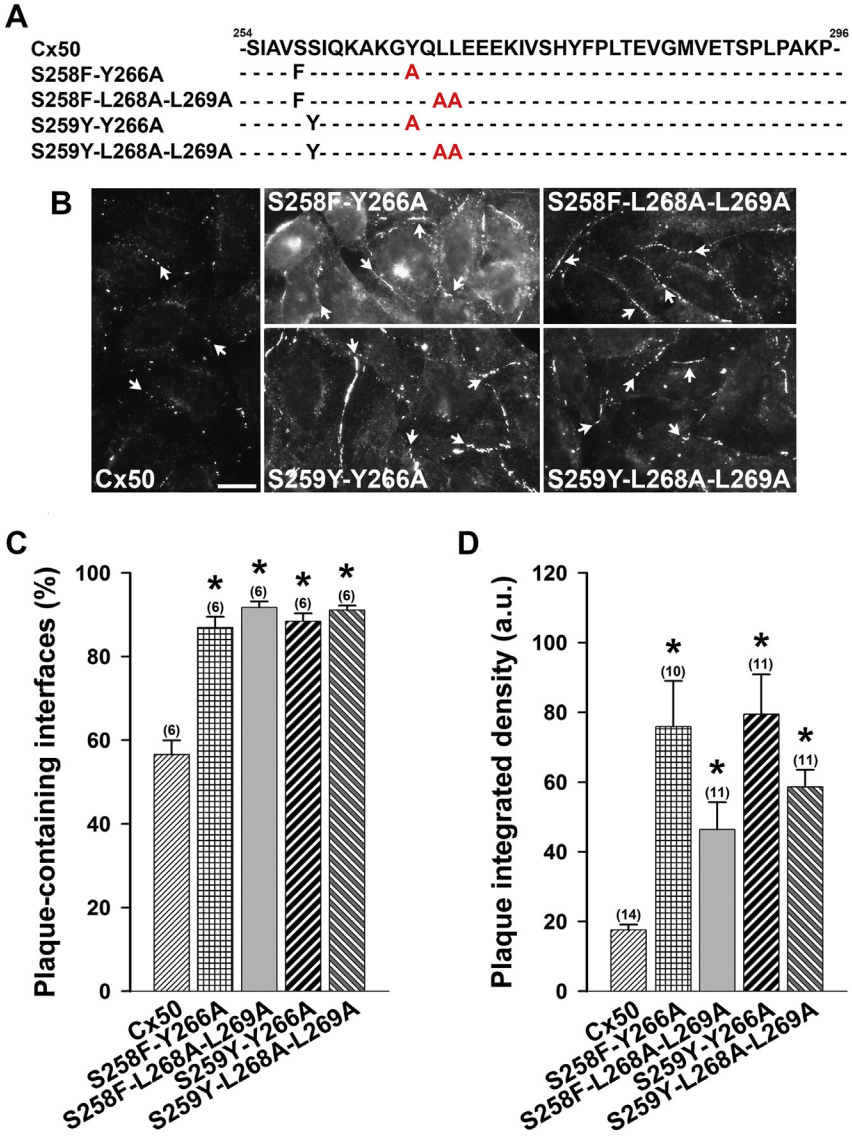

Figure 5. Mutation of the Y-based sorting signal improves gap junctional plaque formation. *A*, the amino acid sequence of wild-type Cx50 from amino acid 254 until amino acid 296 is shown at the *top*. Underneath is a graphical representation of the amino acids substituted by alanine (shown in *red*) on the backbone of the cataract mutants, Cx50S258F and Cx50S259Y, to disrupt the tyrosine-based sorting signal, Y266A and L268A–L269A. *B*, photomicrographs show the distribution of immunoreactive Cx50 in HeLa cells stably transfected with Cx50, Cx50S258F–Y266A (S258F–Y266A), Cx50S258F–L268A–L269A (S258F–L268A–L269A), Cx50S259Y–Y266A (S259Y–Y266A), or Cx50S259Y–L268A–L269A (S259Y–L268A–L269A). *Arrows* point to gap junctional plaques at plasma membranes interfaces. The scale bar represents 16 μm. *C*, graph shows the percentage of cell interfaces that contained gap junctional plaques in HeLa-Cx50, HeLa-Cx50S258F–Y266A, HeLa-Cx50S258F–L268A–L269A, HeLa-Cx50S259Y–Y266A, and HeLa-Cx50S259Y–L268A–L269A cells. *D*, graph depicts the integrated density of the gap junctional plaques in HeLa-Cx50, HeLa-Cx50S258F–Y266A, HeLa-Cx50S258F–L268A–L269A, HeLa-Cx50S259Y–Y266A, and HeLa-Cx50S259Y–L268A–L269A in arbitrary units (a.u.). Data are presented as the mean (bar) + SEM (error bar). Significant differences *versus* HeLa-Cx50 cells are indicated by *asterisks* in *C* and *D*. The number of independent determinations (statistical n) is indicated within parentheses. Cx50, connexin50.

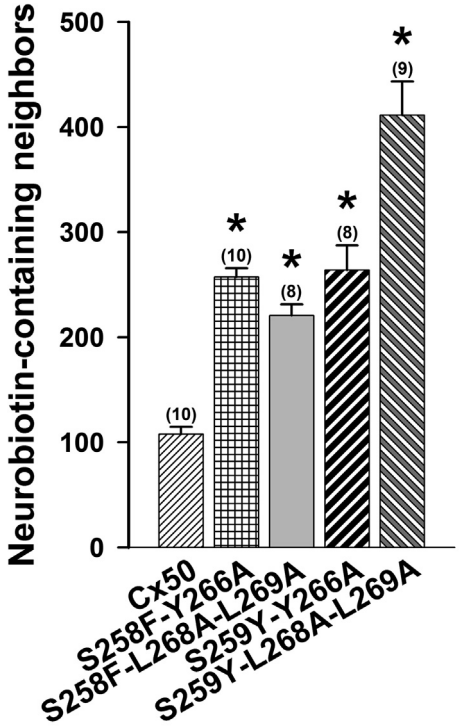

Figure 6. Mutation of the Y-based sorting signal improves intercellular transfer. Bar graph shows the quantification of intercellular transfer of neurobiotin in HeLa cells stably transfected with Cx50, Cx50S258F–Y266A, Cx50S258F–L268A–L269A, Cx50S259Y–Y266A, or Cx50S259Y–L268A–L269A. The results are presented as mean (bar) + SEM. *Asterisks* indicate significant differences *versus* HeLa-Cx50 cells. The number of microinjected cells is indicated within parentheses. Cx50, connexin50.

determined for wild-type Cx50 gap junctional plaques. After the alanine substitutions for L268 and L269 in Cx50S258F and Cx50S259Y, the integrated densities were, respectively, 2.6 and 3.3 times the value in wild-type Cx50 (Fig. 5*D*).

To test gap junction function in the Y266A or L268A–L269A substitution mutants, we determined intercellular transfer of microinjected neurobiotin in the HeLa cell transfectants. All these mutants allowed neurobiotin transfer to at least twice the number of cells in wild-type Cx50 transfectants (Fig. 6). While HeLa cells expressing wild-type Cx50 transferred neurobiotin to an average of 108 cells, HeLa-Cx50S258F–Y266A cells transferred to 257 cells, HeLa-Cx50S258F–L268A–L269A cells transferred to 221 cells, HeLa-Cx50S259Y–Y266A cells transferred to 264 cells, and HeLa-Cx50S259Y–L268A–L269A cells transferred to 411 cells.

Discussion

In this study, we have demonstrated that the cataract-linked mutants, Cx50S258F and Cx50S259Y, support little or no intercellular communication because of the scarcity of gap junctional plaques present at steady state. This loss of function results from exposure of a tyrosine-based sorting signal and degradation of the protein in the lysosome. Only small amounts of the mutant protein are present in gap junctional plaques where they support a low level of intercellular communication. The levels of the mutant protein are more sensitive to inhibition by lysosomotropic amines (chloroquine and NH_4Cl) than the levels of wild-type Cx50, suggesting increased participation of the lysosome in the degradation of the cataract-linked mutant proteins.

Mass spectrometry studies have shown that S258 and S259 in Cx50 are phosphorylated in lenses (16–19). Phosphorylation is a post-translational modification that has been implicated in regulating several steps of the life cycle of connexins, including targeting the protein to the plasma membrane, gating of gap junction channels, internalization of gap junctions, and protein degradation (reviewed in Ref. (23)). Substitution of aspartic acid for S258 or S259 (to add a fixed negative charge mimicking phosphorylation) reverted (if not overshot) the effects of Cx50S258F and Cx50S259Y on connexin levels, gap junctional plaque formation, and intercellular communication. Gap junctional plaques are more abundant, and gap junctional coupling is greater when these positions are occupied by serine or by aspartic acid (mimicking phosphorylation), suggesting the requirement of a negative cloud of electrons at these positions to target the protein to the plasma membrane and/or to stabilize gap junctional plaques; the stronger the electron cloud (as in the aspartate substitution mutants), the stronger the protective effect against targeting the protein to the lysosome for degradation.

Our results suggest that the absence of the phosphorylatable serine residues at positions 258 and 259 in the cataract-linked Cx50 mutants leads to exposure of a sorting signal that targets the protein for lysosomal degradation with a consequent reduction in the cellular levels of Cx50 and the abundance of gap junctional plaques, which contain intercellular channels. We identified the amino acid sequence YQLL (amino acids 266–269) as this sorting signal. It conforms to the tyrosine-based sorting signal of the YXXΦ type that is recognized by the adaptor protein (AP) complexes (reviewed in Ref. (22)). Indeed, mutation of Y266 (an absolute requirement for this type of signal) or L268–L269 to alanines in Cx50S258F and Cx50S259Y significantly improved the number of gap junctional plaques and function. We previously reported increased Cx50 levels and intercellular communication in HeLa cells stably expressing a Cx50 construct truncated after amino acid 255 (as compared with HeLa cells expressing wild-type Cx50) (9). These changes in the truncated Cx50 might also be explained by the elimination of the tyrosine-based sorting signal.

Although the present study is the first time that a disease-associated mutation in a connexin has revealed the presence of a Y-based sorting signal, the presence of tyrosine-based sorting signals was previously predicted from the sequences of several connexins (24). Two studies of site-directed Cx43 mutants have shown the importance of YAYF (amino acids 265–268) and YKLV (amino acids 286–289) for Cx43 gap junction endocytosis and turnover (25, 26). Both classical (AP-2) and alternative (Disabled-2, Dab2) plasma membrane clathrin APs have been implicated in the tyrosine-based signal-dependent internalization of Cx43 gap junctions (26). Considering the large body of evidence demonstrating that

YXXØ signals in many other proteins are recognized by the AP complexes (reviewed in Ref. (22)) and the studies of Cx43, it is likely that clathrin APs are involved in internalization of Cx50 *via* interaction with the YQLL sorting signal. It has been reported that amino acids surrounding the Y-based sorting signal modulate its activity. Interestingly, glycine (the amino acid preceding the YKLV signal in Cx43 and preceding the YQLL signal in Cx50) has been implicated in targeting proteins containing tyrosine-based sorting signals to the lysosome (22).

Taken together with the evidence that S258 and S259 are phosphorylated in the lens (16–19), our study suggests a mechanism for lysosomal targeting and degradation of the mutants. We hypothesize that the carboxyl terminus of wild-type Cx50 (containing phosphorylated serine at position 258 or 259) adopts a conformation that hides the Y-based sorting signal or hinders access of the lysosomal targeting/internalization machinery (Fig. 7*A*). In contrast, in the cataract-linked mutants, Cx50S258F and Cx50S259Y, the absence of a serine at one of these sites prevents phosphorylation and exposes the Y-based sorting signal (Fig. 7*B*), leading to lysosomal targeting of the connexin and degradation. It is likely that lysosomal targeting can occur at any time point after the mutant protein is synthesized. Because at a steady state, most of the mutant protein has a perinuclear localization and rarely some of the protein can be detected forming gap junction plaques, it is likely that the cataract-linked Cx50 mutants behave somewhat similarly to the lysosomal-associated membrane protein 1. This protein also contains a Y-based sorting signal and localizes predominantly in the lysosome with low levels at the plasma membrane (27), but unlike lysosomal-associated membrane protein 1, the Cx50 mutants are degraded in the organelle.

In the lens, increased exposure of the YQLL sorting signal because of mutation of S258 or S259 would lead to targeting of Cx50 to the lysosome and its degradation. Because mature lens fiber cells do not contain organelles, degradation of the mutant Cx50 must occur early in the differentiation process of fiber cells, since only the lens epithelial and differentiating fiber cells contain lysosomes. Degradation of Cx50 would greatly reduce its abundance and the functions it supports. The human cataracts associated with these mutants are nuclear or nuclear pulverulent (*i.e.*, they localize to the center of the lens). This suggests that the most important lost function is intercellular communication, since the lens center is highly dependent on the lens circulation of water and solutes (in which gap junctions play a crucial role). Loss of Cx50 may also induce alterations in structure and integrity of fiber cells in the human lens as seen in Cx50 knockout mice, where such changes have been ascribed to the absence of Cx50's contribution to cell adhesion (28, 29). Significant decreases in fiber cell gap junctional coupling have been reported in Cx50D47A mice and homozygous Cx50-null mice (30–32). In people carrying the Cx50S258F and Cx50S259Y mutations, the cataracts are inherited as autosomal dominant traits (13–15). However, heterozygous Cx50 knockout lenses (which have 50% of the normal levels of Cx50) are transparent (28, 33). The dominant inheritance pattern of the cataracts in individuals carrying the Cx50S258F or Cx50S259Y mutations suggests that these mutants cause a reduction in Cx50 levels and function by more than 50%. This could result through formation of mixed oligomers between the Cx50 mutants and wild-type Cx50. Although wild-type Cx50 in mixed oligomers could potentially rescue trafficking of the mutants to the plasma membrane, these assemblies could be rapidly internalized because of the exposure of the YQLL signal. Thus, it is much more likely that the mutant Cx50 in mixed hexamers causes degradation of wild-type Cx50 leading to disease.

Our studies have revealed the importance of phosphorylation sites that work in conjunction with a Y-based sorting signal. When serine 258 or 259 is phosphorylated, it masks the Y-based sorting signal increasing stability of Cx50 in gap junction plaques. Unphosphorylatable amino acid residues (other than phosphorylation mimics) at these positions lead to exposure of the sorting signal and degradation of the protein. The association of Cx50S258F and Cx50S259Y with cataracts (13–15) implies that serine phosphorylation at these sites and the Y-based sorting signal function together *in vivo* and have a central importance in the mechanism by which these mutants lead to disease. Since other connexins/membrane proteins contain phosphorylation sites and Y-based sorting signals, it is possible that some of their mutations lead to pathologies *via* a similar mechanism.

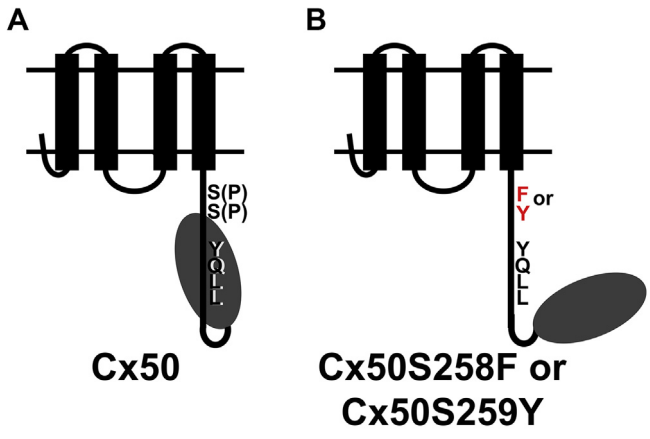

Figure 7. Diagram illustrating the masking or exposure of the C terminus YQLL motif in Cx50. *A*, schematic representation of a monomer of wild-type Cx50. Phosphorylated serine (S(P)) at position 258 or 259 conceals the YQLL sorting signal. *B*, diagrammatic representation of a Cx50S258F or Cx50S259Y monomer. The lack of phosphorylated serine at position 258 or 259 leads to a conformational change that exposes the YQLL sorting signal. Cx50, connexin50.

Experimental procedures

Generation of Cx50 constructs

Cx50 constructs were generated by PCR using High Fidelity Phusion DNA polymerase (New England BioLabs). Primers were designed in opposite directions to incorporate the desired mutations into the PCR product. The different mutants were obtained using the coding region of the wild-type human *GJA8*

gene subcloned into pSFFV-neo as the template (34) and the following primers:

Cx50S258F: sense, CTCCATCCAGAAAGCCAAGGGCTATCAG; antisense, AAGACAGCAATGGAGTGGAGGGATTTCTC

Cx50S259Y: sense, CATCCAGAAAGCCAAGGGCTATCAGCTC; antisense, TAGGAGACAGCAATGGAGTGGAGGGA

Cx50S258D: sense, CTCCATCCAGAAAGCCAAGGGCTATCAG; antisense, TCGACAGCAATGGAGTGGAGGGATTTC

Cx50S259D: sense, CTCCATCCAGAAAGCCAAGGGCTATCAG; antisense, TCGGAGACAGCAATGGAGTGGAGGGA

The following constructs were obtained using Cx50258F or Cx50259Y, respectively, subcloned into pSFFV-neo as the template and primers:

Cx50258FΔ261–279 or Cx50259YΔ261–279: sense, CCCTTGACCGAGGTTGGGATGG

antisense, GATGGAGAAGACAGCAATGGAGTGGAGG

Cx50S258F–Y266A or Cx50S259Y–Y266A: sense, GCACAGCTCCTAGAAGAAGAGAAAATCG

antisense, GCCCTTGGCTTTCTGGATGGA

Cx50S258F–Y278A or Cx50S259Y–Y278A: sense, TTCCCCTTGACCGAGGTTGG

antisense, AGCGTGGGAAACGATTTTCTCTTCTTCT

Cx50S258F–L268A–L269A or Cx50S259Y–L268A–L269A: sense, GCAGAAGAAGAGAAAATCGTTTCCCACT

antisense, TGCCTGATAGCCCTTGGCTTTC

All constructs were fully sequenced at the Cancer Research Center DNA Sequencing Facility of the University of Chicago to ensure that PCR amplification did not introduce random mutations.

Cell culture

HeLa cells were grown in minimal essential medium supplemented with nonessential amino acids, 10% fetal bovine serum, 2 mM glutamine, 100 units/ml penicillin G, and 10 μg/ml streptomycin sulfate. Cells at ∼50% confluence were transfected with wild-type or mutant Cx50 in pSFFV-neo using Lipofectin following the manufacturer's directions (Life Technologies). To obtain stably transfected cells, clones were selected by their resistance to 1 mg/ml geneticin (Thermo Fisher Scientific). To ascertain expression, we screened many clones for wild-type Cx50, Cx50S258F, Cx50S259Y, Cx50S258D, and Cx50S259D by immunofluorescence. All clones expressing the same construct showed a similar distribution of the connexin. We analyzed ten clones of HeLa-Cx50, six clones of HeLa-Cx50S258F, nine clones of HeLa-Cx50S258D, six clones of HeLa-Cx50S259Y, and nine clones of HeLa-Cx50S259D.

Cell treatments

Cells were grown to approximately 80% confluence. Then, the culture growth medium was replaced with normal growth medium containing the corresponding solvent, 2 μM epoxomicin (in dimethyl sulfoxide), 100 μM chloroquine (in water), 20 mM NH_4Cl (in water), or 4 μg/ml brefeldin A (in ethanol) and incubated for 4 h.

Immunofluorescence

Cells were cultured on glass coverslips until they reached ∼80% confluence. Then, they were fixed in 4% paraformaldehyde in PBS for 15 min and subjected to immunofluorescence using previously characterized rabbit polyclonal anti-Cx50 antibodies directed against the carboxyl terminus of Cx50 (amino acids 231–433) (34) or mouse monoclonal anti-Golgi 58K (G2404; Sigma) followed by Cy3-conjugated goat anti-rabbit immunoglobulin G (IgG) antibodies (Jackson ImmunoResearch) or Alexa488 goat anti-mouse IgG (Jackson ImmunoResearch) as described previously (34). Specimens were studied with a Zeiss Plan Apochromat 40× objective (numerical aperture of 1.0) in an Axioplan 2 microscope (Carl Zeiss) equipped with a mercury lamp. Images were acquired with a Zeiss AxioCam digital camera using Zeiss AxioVision software; light intensity and exposure time were kept constant for all images within an experiment. Within each experimental set of samples, the exposure time chosen was that required for the construct having the highest signal intensity (*i.e.*, Cx50S258D, Cx50S259D, Cx50S258F–Y266A, and/or Cx50S259Y–Y266A). Photographic fields were chosen at random. Data analysis was performed independently under blinded conditions by two different investigators, who had not taken the pictures. The number of interfaces containing gap junctional plaques and the integrated density (area × mean gray value) of gap junctional plaques in cells stably transfected with each DNA construct were quantified using ImageJ (35). The highest mean gray value obtained for a gap junction plaque was 137. Six different images (containing up to 45 interfaces each) were analyzed to obtain the number of plaque-containing interfaces. Data are presented as the percentage of the interfaces in each image that contained gap junctional plaques. A minimum of eight images containing up to 16 gap junctional plaques were analyzed to obtain gap junctional plaque integrated density. The results are reported in arbitrary units. Data were compiled from three independent experiments and analyzed for statistical significance using Student's *t* test. Graphs were prepared using SigmaPlot, version 10.0 (Systat Software, Inc). Data are presented as mean + SEM. Figures were assembled using Photoshop CS3 Extended (Adobe Systems, Inc).

Immunoblotting

Cells at 80 to 90% confluence cultured on plastic dishes of 100 mm were rinsed twice with PBS (pH 7.4), harvested in PBS, 4 mM EDTA, 2 mM PMSF, and cOmplete EDTA-free protease inhibitor mixture (Roche Applied Science) and centrifuged at 13,000*g* for 5 min. Pellets were resuspended in harvesting buffer and sonicated. To assess levels of Cx50, aliquots from cell homogenates containing 20 μg of protein were

subjected to immunoblotting. After confirming equivalence of protein loading and transfer by staining the membranes with the Pierce Reversible Protein Stain Kit for polyvinylidene fluoride membranes (Thermo Fisher Scientific) or Ponceau S, membranes were incubated with previously characterized rabbit polyclonal anti-Cx50 antibodies (34) followed by peroxidase-conjugated goat anti-rabbit IgG antibodies (Jackson ImmunoResearch) as previously described (36, 37). Binding of the secondary antibodies was detected using ECL (GE Healthcare). Full-length images of the membranes after protein staining and immunoblotting with anti-Cx50 antibodies are presented in Figs. S7–S10. Fig. S9 demonstrates that the band migrating between 72 kDa and 95 kDa detected in Cx50 immunoblots is nonspecific.

To confirm that epoxomicin inhibited the proteasome, membranes were stripped of antibodies using Restore Plus Western Blot Stripping Buffer (Thermo Fisher Scientific) at room temperature for 20 min and then incubated with anti-ubiquitin (P4D1) antibodies (sc-8017; Santa Cruz Biotechnology, Inc) followed by peroxidase-conjugated anti-mouse IgG antibodies (Jackson ImmunoResearch).

The immunoreactive bands were quantified by densitometry after drawing a rectangular box that encompassed each band using Adobe Photoshop CS3 (Adobe Systems, Inc). The box size used to quantify the immunoreactive band was kept constant for all lanes in an individual blot. The same size box was used to obtain a background value in each lane and correct the integrated band density as previously performed (38). The results are reported in arbitrary units. Graphs were prepared using SigmaPlot 10.0. Statistical analysis was performed using Student's *t* test. Figures were assembled using Photoshop CS3 Extended (Adobe Systems, Inc). Data are presented as mean + SEM.

Reverse transcription quantitative PCR

Cells at about 80% confluence were harvested in QIAzol Lysis Reagent (Qiagen), and the RNA was purified using the miRNeasy Mini Kit (Qiagen). RNA concentrations were determined using a Denovix DS11 spectrophotometer (DeNovix, Inc). Complementary DNA was synthesized using the QuantiTect Reverse Transcription Kit (Qiagen). Quantitative PCR was performed on a 7500 Fast Real-Time PCR System (Applied Biosystems) using a complementary DNA aliquot, Fast SYBR Green Master Mix (Life Technologies, Inc) and a set of B2M (Real Time Primers) or Cx50 (sense 5′-TGCTGAGGACCTACATCTGC-3′; antisense, 5′-CGAAGCAGTCCACCACATTG-3′) primers. These primer sets had an efficiency that was within a 95% confidence value, and they did not produce primer dimers as assessed by the melting curve. All reaction mixes contained equal amounts of RNA. Each sample was run in triplicate in any one of three independent experiments. The transcript for the housekeeping gene, B2M, was used to normalize the relative levels of mRNA among the different HeLa transfectants. Graphs were prepared using SigmaPlot, version 10.0. Data are reported as the geometric mean of the Cx50 levels in the mutant HeLa cell transfectants compared with those in the HeLa-Cx50 cells.

Intercellular communication assays

Electrophysiological studies

To measure gap junctional coupling, the DNA constructs were subcloned into the RNA expression vector, SP64TII. The plasmids were linearized with SalI, and capped RNAs were synthesized using the mMessage mMachine SP6 *in vitro* transcription kit (Ambion) according to the manufacturer's instructions. The amount of RNA was quantified by measuring the absorbance at 260 nm.

Xenopus oocytes were injected with connexin RNA. After 18 h, oocytes were devitellinized and paired as previously described (39). To measure the junctional conductance, cell pairs were studied using the dual two-microelectrode technique (40). Double two-microelectrode voltage clamp experiments were performed using GeneClamp 500 (Molecular Devices) and an Axoclamp 2B (Axon Instruments) as previously described (41). Pulse generation, data acquisition, and analysis were conducted using a personal computer running pCLAMP, version 9.0 (Molecular Devices) and a Digidata 1322A data acquisition system (Molecular Devices). Both cells of the pair were initially held at −40 mV and 5 mV steps were applied to one cell while holding the second cell at −40 mV. The junctional conductance (g_j) equals I_j/V_j, where $V_j = V_{cell\ 2} - V_{cell\ 1}$. Microelectrodes were filled with 3 M KCl (pH 7.4) and had resistances of 0.2 to 2 MΩ. The bath solution was modified Barth's solution. All the experiments were performed on oocytes previously injected with antisense Cx38 oligonucleotides to ensure that the observed currents were not caused by the expression of endogenous Cx38 (42). All the experiments were performed at room temperature (20–22 °C). Data were analyzed for their statistical significance using the unpaired Student's *t* test or Mann–Whitney rank sum test.

Neurobiotin transfer

HeLa cells were cultured on glass coverslips until they reached 90–95% confluence. Then, one cell within a cluster was microinjected with a solution containing 5% Lucifer yellow (charge: −2; molecular weight: 444.4; used to identify the injected cell, because Cx50 shows limited permeability to this dye) and 9% neurobiotin (charge: +1; molecular weight: 287.2; Vector Laboratories) for 1 min using a picospritzer (model PLI-188; Nikon Instruments, Inc). After allowing the microinjected gap junction tracers to diffuse to neighboring cells for 5 min, cells were fixed in 4% paraformaldehyde for 15 min and incubated with Cy3-streptavidin conjugate to allow detection of neurobiotin by fluorescence microscopy as previously described (9). The extent of neurobiotin intercellular transfer was determined by counting the number of adjacent cells containing the tracer. The number of microinjected clusters for cells expressing the different constructs ranged from 6 to

11. Data are presented as mean + SEM. Statistical analysis was performed using Student's *t* test.

Statistical analysis

Data are expressed as mean + SEM. They were analyzed for statistical significance using Student's *t* test or Mann–Whitney rank sum test. A p value of ≤0.05 was considered significant.

Data availability

All data are contained within the article and supporting information.

Supporting information—This article contains supporting information.

Author contributions—P. J. M., E. C. B., and V. M. B. conceptualization; P. J. M. and V. M. B. validation; P. J. M., K. W., H. M., L. E., and V. M. B. formal analysis; P. J. M. and J.-J. T. investigation; V. M. B. writing–original draft; P. J. M., L. E., E. C. B., and V. M. B. writing–review & editing; P. J. M. and V. M. B. visualization; L. E. and V. M. B. supervision; E. C. B. project administration; L. E., E. C. B., and V. M. B. funding acquisition.

Funding and additional information—This work was supported by the National Institutes of Health grants (R01-EY030914 [to E. C. B. and V. M. B.] and R01-EY026902 [to L. E.]). K. W. was supported by the Ted Mullins Fund for Cancer Research. H. M. was supported by a Jeff Metcalf Fellowship from the University of Chicago. The content of this article is solely the responsibility of the authors and does not necessarily represent the official views of the National Institutes of Health.

Conflict of interest—The authors declare that they have no conflicts of interest with the contents of this article.

Abbreviations—The abbreviations used are: AP, adaptor protein; Cx46, connexin46; Cx50, connexin50; IgG, immunoglobulin G.

References

1. Delmar, M., and Makita, N. (2012) Cardiac connexins, mutations and arrhythmias. *Curr. Opin. Cardiol.* **27**, 236–241
2. Srinivas, M., Verselis, V. K., and White, T. W. (2018) Human diseases associated with connexin mutations. *Biochim. Biophys. Acta Biomembr.* **1860**, 192–201
3. Ehrlich, A., Molica, F., Hautefort, A., and Kwak, B. R. (2021) Lymphatic connexins and pannexins in health and disease. *Int. J. Mol. Sci.* **22**, 5734
4. Mathias, R. T., Kistler, J., and Donaldson, P. (2007) The lens circulation. *J. Membr. Biol.* **216**, 1–16
5. Mathias, R. T., White, T. W., and Gong, X. (2010) Lens gap junctions in growth, differentiation, and homeostasis. *Physiol. Rev.* **90**, 179–206
6. Berthoud, V. M., Gao, J., Minogue, P. J., Jara, O., Mathias, R. T., and Beyer, E. C. (2020) Connexin mutants compromise the lens circulation and cause cataracts through biomineralization. *Int. J. Mol. Sci.* **21**, 5822
7. Berthoud, V. M., and Ngezahayo, A. (2017) Focus on lens connexins. *BMC Cell Biol.* **18**, 6
8. Minogue, P. J., Liu, X., Ebihara, L., Beyer, E. C., and Berthoud, V. M. (2005) An aberrant sequence in a connexin46 mutant underlies congenital cataracts. *J. Biol. Chem.* **280**, 40788–40795
9. Minogue, P. J., Beyer, E. C., and Berthoud, V. M. (2013) A connexin50 mutant, CX50fs, that causes cataracts is unstable, but is rescued by a proteasomal inhibitor. *J. Biol. Chem.* **288**, 20427–20434
10. Liu, Y., Qiao, C., Wei, T., Zheng, F., Guo, S., Chen, Q., Yan, M., and Zhou, X. (2015) Mutant connexin 50 (S276F) inhibits channel and hemichannel functions inducing cataract. *J. Genet.* **94**, 221–229
11. Solan, J. L., and Lampe, P. D. (2009) Connexin43 phosphorylation: Structural changes and biological effects. *Biochem. J.* **419**, 261–272
12. Hervé, J. C., Derangeon, M., Sarrouilhe, D., Giepmans, B. N., and Bourmeyster, N. (2012) Gap junctional channels are parts of multiprotein complexes. *Biochim. Biophys. Acta* **1818**, 1844–1865
13. Hansen, L., Mikkelsen, A., Nürnberg, P., Nürnberg, G., Anjum, I., Eiberg, H., and Rosenberg, T. (2009) Comprehensive mutational screening in a cohort of Danish families with hereditary congenital cataract. *Invest. Ophthalmol. Vis. Sci.* **50**, 3291–3303
14. Gao, X., Cheng, J., Lu, C., Li, X., Li, F., Liu, C., Zhang, M., Zhu, S., and Ma, X. (2010) A novel mutation in the connexin 50 gene (*GJA8*) associated with autosomal dominant congenital nuclear cataract in a Chinese family. *Curr. Eye Res.* **35**, 597–604
15. Chen, J.-H., Qiu, J., Chen, H., Pang, C. P., and Zhang, M. (2014) Rapid and cost-effective molecular diagnosis using exome sequencing of one proband with autosomal dominant congenital cataract. *Eye* **28**, 1511–1516
16. Shearer, D., Ens, W., Standing, K., and Valdimarsson, G. (2008) Post-translational modifications in lens fiber connexins identified by off-line-HPLC MALDI-quadrupole time-of-flight mass spectrometry. *Invest. Ophthalmol. Vis. Sci.* **49**, 1553–1562
17. Wang, Z., and Schey, K. L. (2009) Phosphorylation and truncation sites of bovine lens connexin 46 and connexin 50. *Exp. Eye Res.* **89**, 898–904
18. Wang, Z., Han, J., David, L. L., and Schey, K. L. (2013) Proteomics and phosphoproteomics analysis of human lens fiber cell membranes. *Invest. Ophthalmol. Vis. Sci.* **54**, 1135–1143
19. Myers, J. B., Haddad, B. G., O'Neill, S. E., Chorev, D. S., Yoshioka, C. C., Robinson, C. V., Zuckerman, D. M., and Reichow, S. L. (2018) Structure of native lens connexin 46/50 intercellular channels by cryo-EM. *Nature* **564**, 372–377
20. Berthoud, V. M., Minogue, P. J., Laing, J. G., and Beyer, E. C. (2004) Pathways for degradation of connexins and gap junctions. *Cardiovasc. Res.* **62**, 256–267
21. Falk, M. M., Kells, R. M., and Berthoud, V. M. (2014) Degradation of connexins and gap junctions. *FEBS Lett.* **588**, 1221–1229
22. Bonifacino, J. S., and Traub, L. M. (2003) Signals for sorting of transmembrane proteins to endosomes and lysosomes. *Annu. Rev. Biochem.* **72**, 395–447
23. Lampe, P. D., and Lau, A. F. (2004) The effects of connexin phosphorylation on gap junctional communication. *Int. J. Biochem. Cell Biol.* **36**, 1171–1186
24. Thévenin, A. F., Kowal, T. J., Fong, J. T., Kells, R. M., Fisher, C. G., and Falk, M. M. (2013) Proteins and mechanisms regulating gap-junction assembly, internalization, and degradation. *Physiology (Bethesda)* **28**, 93–116
25. Thomas, M. A., Zosso, N., Scerri, I., Demaurex, N., Chanson, M., and Staub, O. (2003) A tyrosine-based sorting signal is involved in connexin43 stability and gap junction turnover. *J. Cell Sci.* **116**, 2213–2222
26. Fong, J. T., Kells, R. M., and Falk, M. M. (2013) Two tyrosine-based sorting signals in the Cx43 C-terminus cooperate to mediate gap junction endocytosis. *Mol. Biol. Cell* **24**, 2834–2848
27. Williams, M. A., and Fukuda, M. (1990) Accumulation of membrane glycoproteins in lysosomes requires a tyrosine residue at a particular position in the cytoplasmic tail. *J. Cell Biol.* **111**, 955–966
28. White, T. W., Goodenough, D. A., and Paul, D. L. (1998) Targeted ablation of connexin50 in mice results in microphthalmia and zonular pulverulent cataracts. *J. Cell Biol.* **143**, 815–825
29. Gu, S., Biswas, S., Rodriguez, L., Li, Z., Li, Y., Riquelme, M. A., Shi, W., Wang, K., White, T. W., Reilly, M., Lo, W.-K., and Jiang, J. X. (2019) Connexin 50 and AQP0 are essential in maintaining organization and integrity of lens fibers. *Invest. Ophthalmol. Vis. Sci.* **60**, 4021–4032

30. Baldo, G. J., Gong, X., Martinez-Wittinghan, F. J., Kumar, N. M., Gilula, N. B., and Mathias, R. T. (2001) Gap junctional coupling in lenses from α_8 connexin knockout mice. *J. Gen. Physiol.* **118**, 447–456
31. Berthoud, V. M., Minogue, P. J., Yu, H., Schroeder, R., Snabb, J. I., and Beyer, E. C. (2013) Connexin50D47A decreases levels of fiber cell connexins and impairs lens fiber cell differentiation. *Invest. Ophthalmol. Vis. Sci.* **54**, 7614–7622
32. Berthoud, V. M., Gao, J., Minogue, P. J., Jara, O., Mathias, R. T., and Beyer, E. C. (2019) The connexin50D47A mutant causes cataracts by calcium precipitation. *Invest. Ophthalmol. Vis. Sci.* **60**, 2336–2346
33. Rong, P., Wang, X., Niesman, I., Wu, Y., Benedetti, L. E., Dunia, I., Levy, E., and Gong, X. (2002) Disruption of *Gja8* (α8 connexin) in mice leads to microphthalmia associated with retardation of lens growth and lens fiber maturation. *Development* **129**, 167–174
34. Berthoud, V. M., Minogue, P. J., Guo, J., Williamson, E. K., Xu, X., Ebihara, L., and Beyer, E. C. (2003) Loss of function and impaired degradation of a cataract-associated mutant connexin50. *Eur. J. Cell Biol.* **82**, 209–221
35. Schneider, C. A., Rasband, W. S., and Eliceiri, K. W. (2012) NIH Image to ImageJ: 25 years of image analysis. *Nat. Methods* **9**, 671–675
36. Minogue, P. J., Tong, J.-J., Arora, A., Russell-Eggitt, I., Hunt, D. M., Moore, A. T., Ebihara, L., Beyer, E. C., and Berthoud, V. M. (2009) A mutant connexin50 with enhanced hemichannel function leads to cell death. *Invest. Ophthalmol. Vis. Sci.* **50**, 5837–5845
37. Berthoud, V. M., Minogue, P. J., Lambert, P. A., Snabb, J. I., and Beyer, E. C. (2016) The cataract-linked mutant connexin50D47A causes endoplasmic reticulum stress in mouse lenses. *J. Biol. Chem.* **291**, 17569–17578
38. Minogue, P. J., Beyer, E. C., and Berthoud, V. M. (2019) CHOP is dispensable for lens transparency in wild-type and connexin50 mutant mice. *Mol. Vis.* **25**, 535–545
39. Ebihara, L. (1992) Expression of gap junctional proteins in *Xenopus* oocyte pairs. *Methods Enzymol.* **207**, 376–380
40. Spray, D. C., Harris, A. L., and Bennett, M. V. L. (1981) Equilibrium properties of voltage dependent junctional conductance. *J. Gen. Physiol.* **77**, 77–93
41. Xu, X., and Ebihara, L. (1999) Characterization of a mouse Cx50 mutation associated with the *No2* mouse cataract. *Invest. Ophthalmol. Vis. Sci.* **40**, 1844–1850
42. Ebihara, L. (1996) *Xenopus* connexin38 forms hemi-gap-junctional channels in the nonjunctional plasma membrane of *Xenopus* oocytes. *Biophys. J.* **71**, 742–748